Spectroscopic ellipsometry investigations of the thermally induced first-order transition of $RbMn[Fe(CN)_6]$

Edgard Davy Loutete-Dangui,[1] Epiphane Codjovi,[1] Hiroko Tokoro,[2] Pierre Richard Dahoo,[3] Shin-ichi Ohkoshi,[2] and Kamel Boukheddaden[1,*]

[1]*Groupe d'Etudes de la Matière Condensée, CNRS-Université de Versailles/St. Quentin en Yvelines, 45 Avenue des Etats Unis, F78035 Versailles Cedex, France*

[2]*Department of Chemistry, School of Science, The University of Tokyo, 7-3-1, Hongo, Bunkyo-ku, Tokyo 113-0033, Japan*

[3]*Service d'Aéronomie (SA) du CNRS UPMC et UVSQ-IPSL-BP3, Route des Gâtines, 91371 Verrières Le Buisson, France*

(Received 22 January 2008; revised manuscript received 24 June 2008; published 31 July 2008)

We report on detailed spectroscopic ellipsometry investigations on the thermally induced first-order phase transition of rubidium manganese hexacyano-ferrate ($RbMn[Fe(CN)_6]$) pellet sample. This switchable solid shows a cooperative Jahn-Teller distortion coupled with a local charge transfer between Fe and Mn ions. Optical spectra of the real, ε', and imaginary, ε'', parts of the complex dielectric constant have been recorded in the interval of temperature, i.e., 250–350 K, around the transition region and in the optical range of 190–830 nm. Four (two) optical bands have been identified and assigned in the low-temperature (high-temperature) phase, corresponding to the Fe^{II}-CN-Mn^{III} (Fe^{III}-CN-Mn^{II}) state. We performed a quantitative analysis by fitting our spectra with Gauss-Lorentz (GL) line shapes and determined the energy positions, oscillator strengths, and widths of individual transitions, as well as their thermal variation. It has been found that the GL profiles excellently approximate the optical response. Moreover, we observed a significant shift of the metal-ligand charge-transfer band8 upon the thermal transition and correlated it quantitatively to the volume change at the transition. We then derived the coefficient of the volumetric thermal expansion of the title compound and found $\alpha=(\partial V/\partial T)/\bar{V}\simeq 3.0\times 10^{-3}$ K^{-1} in the transition region and $\alpha_T^{LT}\simeq 4.0\times 10^{-5}$ K^{-1} ($\alpha_T^{HT}=8.7\times 10^{-5}$ K^{-1}) in the low-temperature (high-temperature) region, in very good agreement with the reported zero thermal-expansion character of this compound. Finally, from the analysis of the integrated absorption spectra, we derived the thermal hysteresis of the high-temperature fraction, which was found in very good agreement with that of magnetic data recorded on the same sample.

DOI: 10.1103/PhysRevB.78.014303 PACS number(s): 47.51.+a

I. INTRODUCTION

Very interesting new types of phase transitions occurring in molecule-based materials are attracting great attention. In such phase transitions, electrons are directly involved since a change in the electronic state is strongly coupled with a change in the lattice. Representative of such exotic phase transitions are transition-metal cyanides, $A^IM^{II}[N^{III}(CN)_6]$ (A=Na, K, Rb, Cs; M=Mn, Co, Cr; N=Fe, Cr),[1–4] which have been extensively studied and are attracting the renewed interest of materials scientists, because of their thermally induced spin-state transition and their fascinating photomagnetic properties. It is well known that the structure of transition-metal cyanides is constituted by central transition-metal ions surrounded by six cyano (CN-) and forms three-dimensional—M-NC-N—network analogous to the double-perovskite-type transition-metal oxides. In addition, most of the transition-metal cyanides contain considerable nonstoichiometric H_2O molecules, making the structural analysis difficult and affecting in a nontrivial way their physical properties. Among the transition-metal cyanides, ($RbMn[Fe(CN)_6]$) (Refs. 5–14) does not contain extra H_2O molecules and therefore constitutes a suitable example for accurate studies of the thermal properties of this family of switchable charge-transfer solids. Previous x-ray investigations[5] on the title compound have shown the existence of a temperature-induced phase transition from the tetragonal (D_{4h}) to a cubic (O_h) phase around 320 K on heating. The mechanism of this structural phase transition involves two processes: (i) a cooperative charge transfer between Mn and Fe (ii) coupled with a cooperative Jahn-Teller (JT) distortion. More precisely, the low-temperature (LT) phase is of type Mn^{III}-Fe^{II} where Mn^{III} is high spin (HS) (d^4, $S=2$) and the Fe^{II} is low spin (LS) (d^6, $S=0$).

The Jahn-Teller distortion of Mn-N_6 octahedron causes the tetragonal structure[15–18] of the LT phase at 200 K on cooling, while at higher temperature, above room temperature, ($RbMn[Fe(CN)_6]$) becomes face-centered cubic (Fm: $Z=4$),[5,18] reflecting the stability of the HT phase Mn^{II}-Fe^{III} in which Mn^{2+} is HS (d^5; $S=5/2$) and Fe^{3+} is low-spin (d^5; $S=1/2$).[5] In fact, upon the cooperative charge transfer between the two metals, at invariant symmetry group, the obtained state is structurally unstable due to the Jahn-Teller character of Mn ion, which produces a long-range cooperative distortion, leading to a first-order transition, accompanied with a large hysteresis loop. Therefore, the cubic to tetragonal structural transition in this material is considered to be driven by a cooperative charge transfer from the Mn^{2+} to the Fe^{3+} sites, coupled with the JT distortion of Mn ions.

Consistently, Osawa *et al.*[19] showed that the low-temperature valence state is HS Mn^{3+} (d^4; $S=2$)-LS Fe^{2+} (d^6; $S=0$) based on their x-ray data and optical-absorption spectra. In the next study of the present work, we denote the high-temperature cubic phase and the low-temperature tetragonal phase as HT and LT phases, respectively. Consequently we expect a large difference between the electronic

states of the HT and LT phases to be evidenced by spectroscopic ellipsometry (SE). Indeed, SE is a powerful technique, well adapted to investigate the electronic and optical changes[20–22] as well as to measure the thickness of thin films.

A previous report by Ohkoshi *et al.*[23] showed the dielectric constant of $(RbMn[Fe(CN)_6])$, observed by SE only in the LT and HT phases and only in the visible region of 400–800 nm. In the present work, we examine the thermal dependence of the dielectric constant in a large interval of temperature below and above the transition temperature, including the transition region (250–383 K), in the extended spectral range of 190–830 nm. Our aim is to correlate the thermal behavior of ellipsometric spectra with the magnetic and x-ray data and to demonstrate how accurate is SE in the investigations of the thermal transitions in switchable solids. Recently, Loutete-Dangui *et al.*[24] showed the first application of the SE as a relevant technique allowing to investigate the thermal properties of the spin-crossover (SC) sample $[Fe(NH2-trz)_3]Br_2$. In particular, SE was able to find out the thermal hysteresis loop of the sample, in very good agreement with that obtained by magnetic measurements.

In this paper, we report on the application of the SE on cooperative Jahn-Teller switchable solids, characterizing quantitatively the charge-transfer transition in $(RbMn[Fe(CN)_6])$ pellet sample, for which there is no visible change in color between the LT and HT phases. The paper is organized as follows. In Sec. II, we present the experimental procedure; in Sec. III, we present the optical spectra obtained at different temperatures and discuss the thermal behavior of the dielectric constants in relation with the cooperative charge transfer leading to a first-order transition. In particular, we fitted our spectra with Gauss-Lorentz line shapes and determined the energy positions, oscillator strengths, and widths of individual transitions at various temperatures in the heating and cooling modes. These results are discussed in Sec. IV. Section V is devoted to the comparison of SE data with that of magnetism performed at this end. We also propose an equation of state for the present phase transition, leading to find the experimental hysteresis loop. In Sec. VI, we end with a conclusion.

II. EXPERIMENTAL SECTION

Pellets of $(RbMn[Fe(CN)_6])$ sample with diameter of 5 mm and thickness of ~1 mm were prepared by pressing the powder under 10 kbar for 1 min using an optical polished piston in order to avoid problems of scattering of the ellipsometric signal, induced by the roughness of the surface. SE is based on measurements of the polarization of a beam of light reflected from the surface of the sample at a known angle of incidence. Two ellipsometric angles, ψ and Δ, are measured as functions of wavelength and the angle of incidence. These parameters are related to the ratio of the reflection coefficients of the sample, r_p and r_s, respectively, associated with *p*-polarized (parallel to the plane of incidence) and *s*-polarized (perpendicular to the plane of incidence) lights,[25] given by

$$\rho = r_p/r_s = \tan(\psi)\exp(i\Delta). \tag{1}$$

The complex refractive index $\tilde{n}=n+ik$ is derived using the well-known semi-infinite model,[21] well adapted here, due to the large thickness of our sample, which gives

$$n + ik = n_0 \sin\phi_0 \sqrt{1 + \left(\frac{1-\rho}{1+\rho}\right)^2 \tan^2\phi_0}, \tag{2}$$

where n_0 (=1) and $\phi_0=70°$ are, respectively, the refractive index of the vacuum and the incidence angle taken here near the Brewster angle.

The real, ε', and imaginary, ε'', parts of the dielectric constant are related to the dispersion and extinction coefficients given by

$$\varepsilon'(\lambda) = n^2 + k^2 \quad \text{and} \quad \varepsilon''(\lambda) = 2n(\lambda)k(\lambda). \tag{3}$$

Equations (1)–(3) link the ellipsometric parameters (ψ,Δ) and the indices n and k or the dielectric constants ε' and ε''.

SE measurements on a $(RbMn[Fe(CN)_6])$ pellet sample have been performed in the wavelength of 190–830 nm using a UVISEL spectroscopic ellipsometer, in which the polarization of light is modulated through a photoelastic device.[26,27] The light source was a 150 W Xe short arc lamp, and calcite prism polarizers were used to polarize the incident beam and to analyze the light beam reflected by the sample.

The temperature of the sample was controlled by a temperature controller (Linkam TMS 94) with a platinum resistor sensor embedded near the surface of the heating-cooling stage, allowing accurate (0.1 K) temperature measurements. The experiments were performed in the temperature range of 225–380 K, and the typical recording times were 3–5 min, which have been taken in order to accumulate the optical spectra. The pellet sample was in a chamber under controlled atmosphere of nitrogen. The light spot on the sample has an ellipsoidal shape with a size is ~1–2 mm, and it probes always the same region of the sample. We have checked that different experiments realized at constant temperature, probing different regions of the sample, gave the same result, which excludes the existence of large temperature gradients during the experiment.

III. RESULTS

We have recorded various spectra of $\Delta(\lambda)$ and $\Psi(\lambda)$ in the range of 250–380 K in the heating and in the cooling modes, from which we derived the thermal evolution of the dielectric constants $\varepsilon'(\lambda,T)$ and $\varepsilon''(\lambda,T)$. In Figs. 1(a) and 1(b), we show the respective wavelength dependence of the ellipsometric parameters Δ and Ψ (in inset) and that of the dielectric constants $\varepsilon''(\lambda)$ and $\varepsilon'(\lambda)$ (in inset) in the LT (at 296 K) and HT (at 380 K) phases.

To analyze the consistency of our experimental results, we first checked in both states, i.e., LT and HT, in which these quantities obey the Kramers-Kronig (KK) relations[28–30] given by

$$\varepsilon'(\omega) = 1 + \frac{2}{\pi} P \int_0^\infty \frac{\omega' \varepsilon''(\omega')}{\omega'^2 - \omega^2} d\omega', \tag{4}$$

and

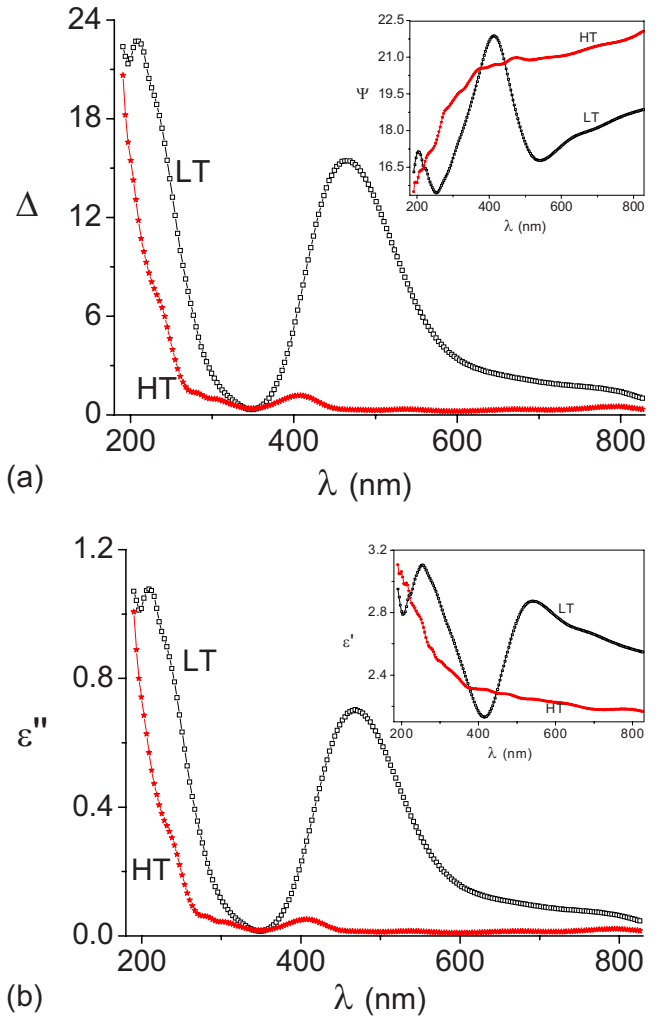

FIG. 1. (Color online) (a) Wavelength dependence of the ellipsometric parameters Δ and ψ (in inset) of ($RbMn[Fe(CN)_6]$) in the HT (383 K, ⋆) and LT (296 K, □) phases near the pseudo-Brewster's angle (70°); (b) wavelength dependence of the dielectric constants ε' and ε' (in insert) in the HT (383 K, ⋆) and LT (296 K, □) phases derived from (a).

$$\varepsilon''(\omega) = -\frac{2\omega}{\pi} P \int_0^\infty \frac{\varepsilon'(\omega') - 1}{\omega'^2 - \omega^2} d\omega', \tag{5}$$

where P is the Cauchy's principal value of the integral, and ω is the frequency. Therefore, starting from the experimental spectra of $\varepsilon''(\lambda)$, as input data, we have calculated $\varepsilon'_{cal}(\lambda)$ using relation (4). Good agreement was obtained between the experimental $[\varepsilon'_{expt}(\lambda)]$ and calculated $[\varepsilon'_{calc}(\lambda)]$ dielectric constants using KK relation, as shown in Fig. 2. In particular, an absorption band centered around 460 nm is found in both phases. In contrast, a discrepancy between $[\varepsilon'_{expt}(\lambda)]$ and $[\varepsilon'_{calc}(\lambda)]$ is observed in the range of 240–300 nm, which does not affect the absorption band in the visible region. This deviation, which is enhanced in the UV region is attributed to the light scattering due to the surface roughness of the pellet sample. A previous ellipsometric study on a pellet of a spin-crossover sample[24] showed a similar effect.

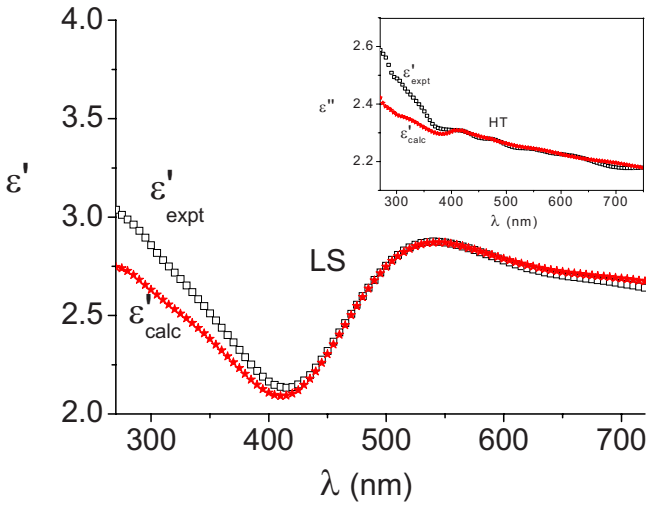

FIG. 2. (Color online) Wavelength dependence of the experimental (□) and the calculated (⋆) dielectric constants ε' using KK relations in the (a) LT and in the (b) HT states. Good agreement is obtained round the absorption region.

Moreover, the study of the whole spectra, obtained in the heating and cooling modes, shown in Fig. 3, evidenced that the latter follow a regular and monotonic behavior with temperature. On the other hand, in the LT state, one main band of absorption was observed in visible region of the absorption spectra. This band is assigned to the association between intervalence and charge-transfer bands.

The ellipsometric spectra contains the following the contributions: (1) the metal-to-metal charge-transfer band, usually denoted intervalence (IT) transfer band, arising from Fe^{II}-Mn^{III} to Fe^{III}-Mn^{II} (and reversibly) transitions, (2) the JT distortion (Mn^{III} *d-d*), (3) metal-to-ligand charge transfer (MLCT) Fe^{II} to CN charge transfer of $[Fe^{III}(CN)_6]$, (4) *d-d* transition of Fe^{III}, (5) and ligand-to-metal charge-transfer

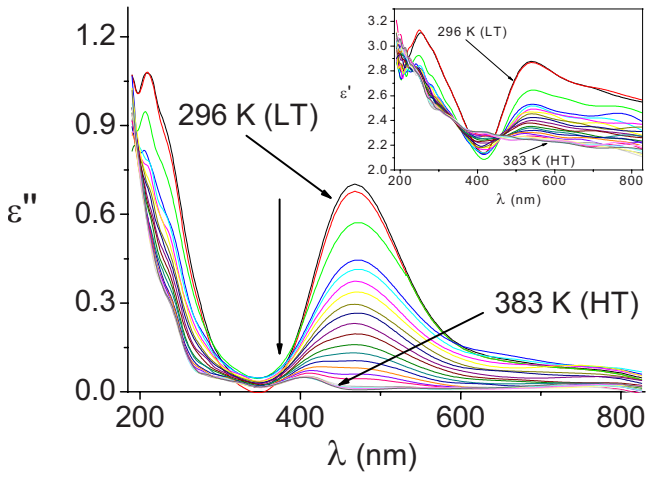

FIG. 3. (Color online) Thermal evolution of $\varepsilon''(\lambda)$ spectra of ($RbMn[Fe(CN)_6]$) in heating from 296 K (LS) up to 383 K (HS). Note the energy shift of the MLCT band and the invariance of the JT band, which is centered around 504 nm. In the inset, shown are the spectra of the real dielectric constant, $\varepsilon'(\lambda)$, at the same temperatures. The temperature increment is 4 K.

(LMCT) transitions, corresponding to CN to Fe^{III}. We have studied the absorption line shape of the obtained spectra in the frame of the Lorentz model.[31,32] Such a model is valid in case of linear dispersive media and describes the dielectric type as a collection of neutral atoms with elastically bound electrons to the nucleus, which gives a set of Lorentz oscillators.

Starting from the macroscopic electric susceptibility of the medium, which writes as[33]

$$\chi_e(\omega) = -\sum_j \frac{N_j e^2/m}{\omega^2 - \omega_j^2 + 2i\delta_j\omega}, \tag{6}$$

where ω_j is the resonance frequency of the jth Lorentz oscillator, δ_j is the associated phenomenological damping constant, and N_j is the associated number of resonant electrons per unit volume interacting with the applied local electric field. The complex dielectric permittivity $\varepsilon(\omega)$ of the medium is given by

$$\varepsilon_L(\omega) = 1 + 4\pi\chi_e(\omega) = 1 - \sum_j \frac{b_j^2}{\omega^2 - \omega_j^2 + 2i\delta_j\omega}, \tag{7}$$

where b_j is the plasma frequency with number density N_j. The complex index of refraction, denoted here $\tilde{n}(\omega)=n(\omega)+ik(\omega)$, is related to the dielectric permittivity $\varepsilon(\omega)$ as

$$\tilde{n}(\omega) = \sqrt{\varepsilon(\omega)} = \left(1 - \sum_j \frac{b_j^2}{\omega^2 - \omega_j^2 + 2i\delta_j\omega}\right)^{1/2}. \tag{8}$$

In the present study, we have chosen to analyze the line shape of the imaginary part of the complex dielectric constant instead of that of the real part, which is less sensitive to the surface roughness and consequently to scattering phenomena.

We use the line shape given in Eq. (7), where the subscript j runs over four and two Lorentz oscillators in the LT and HT phases, respectively. In the LT region, corresponding to $260 < T < 300$ K, the four oscillators—which are shown in Fig. 4(a)—are localized at 685, 508, 457, and 210 nm. The absorption at 685 and 508 nm can be assigned to Mn^{III} d-d transitions, respectively, associated with the Jahn-Teller distorted Mn^{3+} $^5B_{1g} \rightarrow {}^5A_{1g}$ and $^5B_{1g} \rightarrow {}^5B_{2g}$, ^5E_g transitions.[15,34,35] The absorption at 456 nm is identified as the intervalence Fe^{II}-Mn^{III} electron transfer band, and the absorption at 210 nm is assigned to the MLCT band of $[Fe^{2+}(CN)_6]$.[23] However, a detailed analysis shows that this band consists in several overlapping subbands due to the existence of vibronic structure.

In the HT region, associated with the high-symmetry phase, the dielectric constant is well reproduced using two Lorentz oscillators, as seen in Fig. 4(b). The observed absorption peaks are located at 405 and 220 nm, respectively, assigned to the ligand-to-metal charge-transfer bands of $[Fe^{3+}(CN)_6]$, (LMCT1) and (LMCT2).[23] For intermediate temperatures, the optical spectra consist in a combination of HT and LT peaks, weighted by Boltzmann probabilities. In order to analyze the fine structure of the total spectra, we have used a least-square-fit procedure in which we vary the parameters (E_j, b_j, Γ_j) of each Lorentz oscillator in order to minimize the difference between the observed and calculated values of $\varepsilon''(E)$ in the whole temperature range. In each spectrum, we have considered 640 points corresponding to a wavelength step of 1 nm in the interval of 190–830 nm. More than 48 spectra have been accumulated in heating and cooling modes from 380 to 260 K. In order to increase the consistency of our fitting procedure, we have constrained the values of the resonance energies of the different bands at their values obtained in the literature,[15,23,34,35] except that of the MLCT band which shifts with temperature. Practically, we found that the pure Lorentz model does not allow us to reproduce accurately the experimental results. Consequently, we assumed that the resonant energies E_j may fluctuate randomly[36] with the Gaussian probability density,

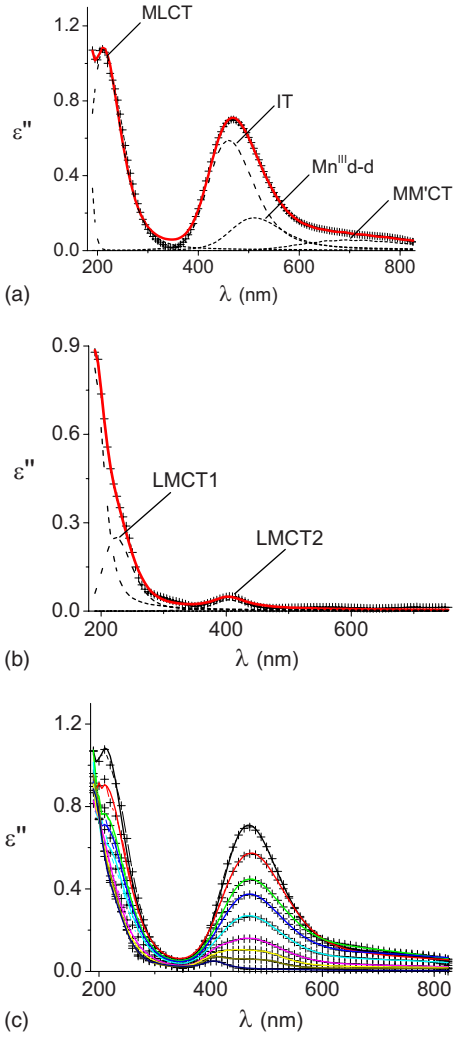

FIG. 4. (Color online) Measured (+) and fitted (solid line) spectra of $\varepsilon''(\lambda)$, obtained using LG profile [Eq. (11)] in (a) the tetragonal (LT phase, $T=296$ K), (b) the cubic (HT phase, $T=383$ K), and (c) at various selected temperatures. The contributions of the individual bands are shown by dashed lines. The number of experimental points has been strongly reduced for clarity reasons.

$$P_G(E_j) = \frac{1}{\sqrt{2\pi}\Gamma_{Gj}} \exp[(E_j - \langle E_j \rangle)^2 / 2\Gamma_{Gj}^2], \tag{9}$$

where $\langle E_j \rangle$ is its mean value and Γ_{Gj} is the standard deviation. These random fluctuations modify the Lorentzian line shapes, and the resulting Lorentz-Gauss (LG) profiles are then obtained by convolution as

$$\varepsilon_{LG}(E) = \frac{1}{\sqrt{2\pi}\Gamma_G} \int_{-\infty}^{+\infty} \varepsilon_L(E) P_G(E_0) dE_0, \tag{10}$$

where $\varepsilon_L(E)$ is the Lorentz contribution to the dielectric constant. Substituting $\varepsilon_L(E)$ by its expression given by Eq. (7), Eq. (10) becomes

$$\varepsilon_{LG}(E) = \varepsilon_\infty + \sum_j \frac{S_j E_j^2}{\sqrt{2\pi}\Gamma_{Gj}} \int_{-\infty}^{+\infty} \frac{e^{-(E_j - x)^2 / 2\Gamma_{Gj}^2}}{x^2 - E^2 - 2i\Gamma_{Lj}E} dx, \tag{11}$$

where ε_∞ is a dielectric constant arising from higher-lying transitions, while the dimensionless parameter S_j is the oscillator strength of the jth band.

It is important to notice that the real and imaginary parts of the dielectric function obey the KK relations and can be computed efficiently using the complex probability function.[37] We have performed a fitting of the experimental spectra at various temperatures with GL profiles by allowing variations of all adjustable parameters of Eq. (11), i.e., S_j, E_j, Γ_{Lj}, and Γ_{Gj}. In the LT phase, more than 300 points were fitted to determine the unknowns, the number of which depends on the state (i.e., LT or HT) of the system. Thus, in the LT (HT) state, four (two) oscillators are considered, leading to fit 16 (8) parameters. However, strong correlations exist between the Lorentzian and Gaussian broadenings, leading to the lack of precision of the linewidths. Remarking that the Gaussian widths are more or less independent of temperature, we fixed them at their averaged value $\Gamma_G \approx 0.23$ eV, obtained from the analysis of all the spectra at different temperatures. In addition, in our fitting procedure, we first fixed the input values of the transition energies at the values obtained in the literature given by 1.81, 2.58, 2.68, 5.93, and 6.58 eV (3.06 and 5.63 eV) for the LT (HT) phase, except that of the UV band. It is also remarked that the contribution of the UV band (MLCT) of the LT phase can be fitted using a single band, independently of that of the visible region (IT and Mn^{III} d-d contributions) due to the presence of a negligible overlapping. Similarly, the IT band at 685 nm also shows a small overlapping with the JT Mn^{III} d-d and therefore can be treated independently, which leads to fit only two parameters (intensity and Lorentz width). Therefore, four fitted parameters (two intensities and two Lorentzian widths) are analyzed, a method which drastically reduces the strong correlations existing between the fitted parameters.

Following this method, the number of fitted parameters (b_j and Γ_{Lj}) in the LT (HT) phase reduces to 8 (4). Once this first step achieved, we set free the energies and we fit them. The procedure is repeated until to obtain the lowest value of $\chi 2 = \Sigma_N^{i=1} [\varepsilon''_{\text{expt}}(E_i) - \varepsilon''_{\text{calc}}(E_i)]^2$, where $\varepsilon''_{\text{expt}}(E_i)$ $[\varepsilon''_{\text{expt}}(E_i)]$ is the calculated (experimental) dielectric constant. The results of the fit in the case of LT and HT phases, are shown in Figs. 4(a) and 4(b). It is evidenced from Fig. 4(c) that the LG model well reproduces the experimental results at all temperatures in the cooling and heating modes. The obtained parameters values with their standard deviation are listed in Table I.

IV. DISCUSSION

Several informations can be derived from the present study. On decreasing temperature, a pronounced decrease in the Lorentzian widths is observed, as seen in Fig. 5, which summarizes the temperature dependences of the oscillator strengths and that of the transition energies.

The broadening of the absorption bands described by the Gaussian and Lorentzian widths may have several physical origins. In addition to the finite temperature-independent lifetime of excited states, which reflects the Heisenberg uncertainty principle, the broadening can be assigned to the existence of local disorder of various origins: existence of water molecule coordinated with Fe atom, instead of cyanide bridge.[38] It is worth noting that such disorder causes the inhomogeneous broadening of the lines (expected to be temperature independent) and may affect the relative energy gap between the LT and HT states. Moreover, a homogeneous broadening can be induced by thermal noise due to lattice and bond-length fluctuations. In the present case, the temperature-dependence analysis of the band widths showed a typical homogeneous broadening, the amplitude of which reaches the value 0.13 eV at ambient temperature, where the total width including inhomogeneous broadening is estimated as 0.8 eV. The thermal dependent part of the effective width originates from Doppler effect, due to the Boltzmann distribution of the velocities, as seen in Fig. 5(a), where the temperature dependence of the central absorption peak width follows the usual Doppler law $\Delta\nu \propto \sqrt{T}$, where T is the absolute temperature. However, the large observed value of the amplitude (0.13 eV) leads to unrealistic atomic velocities, suggesting that the total homogeneous width is made up of a superposition of several Lorentzian lines.

We additionally depicted in Fig. 5(b) the temperature-dependence of the oscillator strengths associated with the different line shapes. There, we found that the oscillator strengths of the IT and Mn^{III} d-d bands, which constitute the "fine structure" of the central band located at 2.65 eV (468 nm), are decreasing functions of temperature and well reproduce the present first-order transition with its hysteresis loop. The decreasing dependence of the oscillator strengths of IT (Fe^{II}–NC-$Mn^{III} \rightarrow Fe^{II}$–NC-$Mn^{III}$ transition) and JT (Mn^{III} d-d) peaks with temperature reflects the Boltzmann population of the HT phase, which is made of Fe^{III}-NC-Mn^{II}. Therefore, these two peaks can be used to estimate the thermal evolution of the HT fraction, as it will be done in Sec. V.

While the central peak does not show significant shift of temperature, it is remarked that the MLCT bands located at 210 nm in the HT phase leads to a blueshift on decreasing temperature. This behavior is mainly due to the large thermal contraction of the metal-ligand distance due to the enhancement of orbital overlapping at low temperature. Conse-

TABLE I. The least-square fit parameters derived from GL analysis $\varepsilon''(\lambda)$ spectra of ($RbMn[Fe(CN)_6]$) for selected temperatures.

T (K)	E_j (eV) [λ (nm)]	S_j	Γ_{Lj} (eV)	Γ_{Gj} (eV)	χ^2
296 (LT)	1.81 (685)	0.24 (8)	0.1 (1)	0.24	0.041
	2.44 (508)	0.81 (5)	0.23 (3)	0.184	
	2.71 (457)	1.86 (3)	0.156 (5)	0.24	
	5.93 (210)	0.444 (6)	0.228 (5)	0.77	
318	1.81 (685)	0.21 (2)	0.29 (5)	0.24	0.016
	2.44 (508)	0.7575 (7)	0.17 (1)	0.184	
	2.71 (457)	1.641 (2)	0.227 (6)	0.24	
	3.06 (405)	0.012 (2)	0.152 (1)	0.202	
	5.93 (210)	0.342 (5)	0.220 (1)	0.77	
328	1.81 (685)	0.20 (6)	0.47 (1)	0.24	0.0086
	2.44 (508)	0.48 (6)	0.15 (5)	0.184	
	2.71 (457)	1.15 (3)	0.25 (1)	0.24	
	3.06 (405)	0.04 (2)	0.154 (1)	0.202	
	5.93 (210)	0.267 (2)	0.211 (1)	0.77	
333	1.81 (685)	0.17 (5)	0.7 (1)	0.24	0.0085
	2.44 (508)	0.34 (3)	0.12 (4)	0.184	
	2.71 (457)	0.84 (3)	0.26 (6)	0.24	
	3.06 (405)	0.06 (2)	0.16 (1)	0.202	
	5.93 (210)	0.242 (2)	0.208 (1)	0.77	
383 (HT)	3.06 (405)	0.21 (2)	0.7 (1)	0.202	0.018
	5.63 (220)	0.145 (2)	0.17 (1)	0.6	

quently, no isobestic point is observed in this system, contrary to the spin-crossover $[Fe(NH_2-trz)_3]Br_2$ solid previously studied[24] by SE and in which there is no charge-transfer, or x-ray, studies, available in the literature. We have reported the energy shift of this band in Fig. 5(c) and obtained a hysteresis behavior.

We now establish a direct correlation between the shift of the experimental MLCT band and the volume expansion upon the transition. Knowing that the unit cell of the title compound contains four Mn ions and its volume in the LT and HT phases, derived from x-ray diffraction analysis,[15,39] is, respectively, 1057 $Å^3$ and 1169 $Å^3$, we derive a relative expansion $\Delta V/V \approx 10\%$ upon the thermal transition. This value is in very good agreement with the obtained relative energy shift $\Delta E/E \approx 12\%$, deduced from Fig. 5(c) in the transition region.

The effect of the strain on the electronic structure of the MLCT band can be interpreted in terms of the deformation-potential theory.[40] Considering only the hydrostatic component of the strain tensor, which affects the energy gap linearly with the strain, it is expected to have $\Delta E \propto \Delta V$, where ΔE (ΔV) is the energy (volume) change. Such relation is also expectable form a vibronic model in the case of isostructural transition. In the present case, we easily derive from Fig. 5(c) that $\Delta E/E \approx 12\%$ in the transition region; the value which is in very good agreement with the relative volume jump $\Delta V/V \approx 10\%$ reported in literature.[8,15] Therefore we adopt the relation $\Delta E/E \approx \Delta V/V$ which is also valid in the LT and HT phases. Consequently, the coefficient of the volumetric thermal expansion, α, can be easily deduced from the ellipsometric data as $\alpha = (\partial V/\partial T)/\bar{V} \approx (\partial E/\partial T)/\bar{E}$.

We have evaluated from Fig. 5(c) the expansion coefficient $\alpha(T)$ and obtained $\alpha_T^{LT} \simeq 4.0 \times 10^{-5}$ K^{-1} and $\alpha_T^{HT} \simeq 8.7 \times 10^{-5}$ K^{-1} in the LT and HT phases, respectively. Such values are in very good agreement with the zero thermal-expansion character of this family of solids, as reported in literature.[41] Indeed, when comparing the above values to that of the SC compound,[42] $Fe(phen)_2(NCS)_2$, for which we found $\alpha_T^{LT} \simeq 1.6 \times 10^{-4}$ K^{-1} and $\alpha_T^{HT} \simeq 1.6 \times 10^{-4}$ K^{-1}, it is evidenced that the $RbMnFe(CN)_6$ is more rigid than the SC compound in both HT and LT phases. The zero thermal expansion of the solid in the LT and HT phases allows us to write the temperature dependence of the unit-cell volume as $V(T) = n_{HT}\delta V + V_{LT}$, where $\delta V = V_{HT} - V_{LT} \approx 28$ $Å^3$ and $V_{LT} = 1057$ $Å^3$ is the volume of the unit cell in the LT phase.

It is also worth remarking that our spectra exhibits two different thermal behavior of the peak positions between the of MLCT (210 nm) and JT optical band (504 nm). Indeed, while the latter shifts with temperature, the energy of the former remains invariant in the cooling and heating mode. We explain the behavior of the JT band by the localized nature of the transition energy, which is exclusively centered

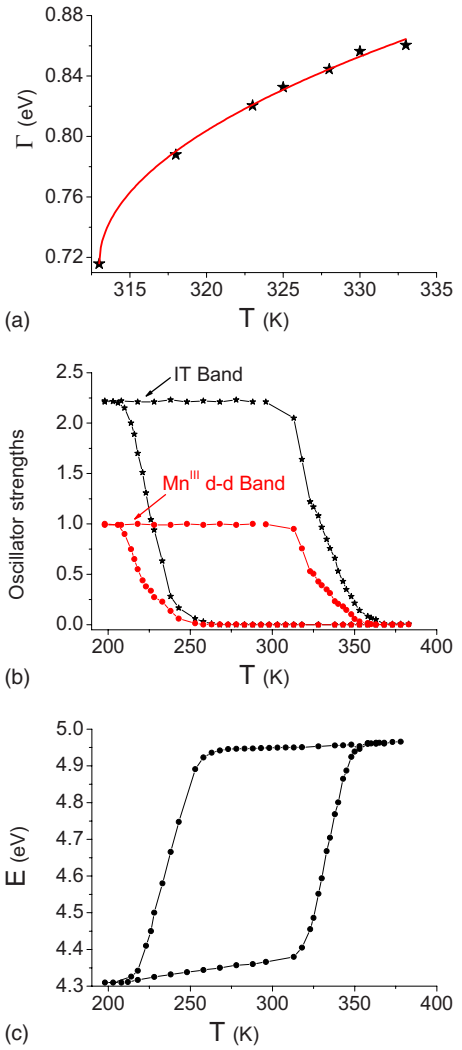

FIG. 5. (Color online) Temperature dependences determined by SE of the width of (a) the experimental central band localized at 468 nm, (b) the oscillator strengths of the IT and Mn^{III} *d-d* bands, and (c) the energy shift of the MLCT band.

on the Mn ion, while it is environment dependent for the MLCT band.

V. COMPARISON BETWEEN ELLIPSOMETRY AND MAGNETISM

Magnetic data recorded on the pellet sample are shown in Fig. 6, where we reported the thermal dependence of the HT fraction, which is the fraction of Mn^{2+} $[Fe^{3+}(CN)_6]$. The obtained results clearly indicate a shift of the hysteresis loop at higher temperature, in comparison with that of the powder sample,[15,43–45] which is the signature of the existence of a residual pressure in the pellet sample, similar to that observed in the SC solid $[Fe(NH_2-trz)_3]Br_2$.[24] Knowing the entropy change at the transition, this residual pressure can be evaluated using the Clapeyron's relation giving the pressure dependence of the transition temperature as $T_{1/2}(p)=T_{1/2}(0)+p\Delta V/\Delta S$, where ΔV (ΔS) is the volume (entropy) change upon the transition. The ratio $\Delta V/\Delta S$ is derived from the

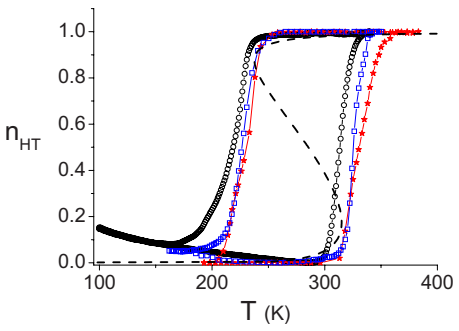

FIG. 6. (Color online) Thermal hysteresis of $(RbMn[Fe(CN)_6])$ with HT fraction derived from magnetic data (○) of the powder sample and of the pellet (□) compared to SE measurements on the same pellet (⋆). The dashed line is the theoretical curve derived from an Ising-type approach.

phase diagram of the powder sample, obtained by reflectivity measurements under pressure, which was found ~24 K/kbar.[46] This ratio can be also determined from the combination of heat-capacity and x-ray measurements. Recent heat-capacity experiments gave an entropy change $\Delta S=54$ J K^{-1} mol^{-1},[47] and the volume change in the molecule—that is, the volume change per Mn ion at the transition was measured $\simeq 28$ $Å^3$ (Refs. 15 and 39)—finally leading to $\Delta V/\Delta S \simeq 30$ K/kbar, a value in good agreement with that reported above. The observed shift of the transition temperature is positive, which denotes the presence of a residual pressure inside the pellet sample, stabilizing the LT phase which has a smaller volume. Quantitatively, we found $\Delta T_{1/2}=T_{1/2}(p)-T_{1/2}(0)\simeq 5$ K, giving rise to a residual pressure $p\simeq 0.19$ kbar. To compare quantitatively magnetic and ellipsometric data, we followed the thermal dependence of the surface of the central experimental absorption band located around $\lambda \approx 468$ nm (JT and IT bands). Assuming a linear dependence between the HT fraction and the absorption area $A(T)$ at temperature T, we write the HT fraction as $n_{HT}(T)=[A(T)-A_{LT}]/(A_{HT}-A_{LT})$; where A_{LT} (A_{HT}) is the $A(T)$ values in the LT (HT) phase. The obtained results are reported in Fig. 6, which clearly indicates an excellent agreement with the magnetic data. A similar procedure, also leading to very good agreement, was used to derive the HT fraction from the thermal evolution of the intensity of the central experimental band $I(T)$ as $n_{HT}(T)=[I(T)-I_{LT}]/(I_{HT}-I_{LT})$, where I_{LT} (I_{HT}) is the value of $I(T)$ in LT (HT) phase. It is also worth mentioning that simple renormalization of the thermal evolution, of the oscillator strengths of the IT and Mn^{III} *d-d* bands, or of the energy shift of the UV band also reproduces properly the thermal dependence of the HT fraction.

One of the most informative quantities extracted from the hysteresis loop is the interaction strength between the molecules, which monitors the existence and the width of the hysteresis loop. Usually to extract such quantity a fitting of the hysteresis loop is made. Here, we want to present a simple method leading to evaluate analytically the interaction parameter, denoted here as J, without any fitting of the data.

We start from the well-known Ising-type model,[17,48] which is not the most adapted model to describe this struc-

tural first-order transition. Indeed, the present phenomenon requires a two-order-parameter description, respectively, associated with the cooperative charge-transfer process and the symmetry change. If we accept the sacrifice of use of the simple Ising-type Hamiltonian, which accounts only for the change in the electronic properties and ignores the structural changes, then the electronic configurations Fe^{II}-Mn^{III} (LT) and Fe^{III}-Mn^{II} (HT) can be, respectively, associated with a two-state fictitious spin operator, $\sigma=-1,+1$. In such simple model, the equation of state giving the relation between the HT fraction, n_{HT}, and temperature writes in the mean-field (MF) approximation[48] as

$$n_{HT}=\frac{1}{2}+\frac{1}{2}\tanh\beta\left[J(2n_{HT}-1)-\Delta+\frac{k_BT}{2R}\Delta S\right], \quad (12)$$

where ΔS is the molar entropy change, Δ is an energy gap, $\beta=\frac{1}{k_BT}$, k_B is the Boltzmann constant, and R is the perfect gas constant.

It is important to notice here that the MF theory gives the same equilibrium states as an Ising-type Hamiltonian with an infinite long-range interactions (Husimi-Temperley model). Thus, the MF approximation misses the correlations between the molecules. In addition, in such description, the interaction parameter J is introduced phenomenologically and assumed to be constant, while it certainly depends on the deformation of the molecular units.[49] Indeed, usually the elastic interactions, and particularly the dipole-dipole interactions ($\propto 1/r^3$) play an important role in the crystal and even they can attractive or repulsive depending on the relative orientation of the elastic dipoles.

To treat the self-consistent Eq. (12), in order to extract analytically the interaction parameter, J, it is necessary to express the temperature T against the HT fraction, n_{HT}. In such case, the upper and lower "transition" temperatures, limiting the width of the hysteresis width, are obtained experimentally. The derivative $\partial T/\partial n_{HT}$, leads to the following relation:

$$\frac{\partial T}{\partial n_{HT}}=J\left[\arg\tanh(2n_{HT}-1)+\frac{\Delta S}{2R}\right]-\frac{J(2n_{HT}-1)-\Delta}{1-(2n_{HT}-1)^2}. \quad (13)$$

Combining Eqs. (13) and (12), and the experimental slope $\partial T/\partial n_{HT}$ at the transition temperature, we arrive to the following formula, connecting the interaction parameter J, with the other parameters of the model as

$$J\simeq k_BT_{1/2}+\frac{k_B\Delta T\times\Delta S}{4R\Delta n_{HT}}. \quad (14)$$

There, $T_{1/2}=2\Delta/(\Delta S/R)\simeq 280$ K is the transition temperature, $\Delta T\simeq 100$ K is the hysteresis width, and $\Delta n_{HT}\simeq 0.9$ is the jump of the HT fraction at the transition temperature. These values extracted from Fig. 6 lead to an enthalpy change at the transition $2\Delta\simeq 1930$ K. Using these values in Eq. (14), we find the interaction parameter value, $J=547$ K. Inserting, these parameter values in Eq. (12), we calculate the theoretical hysteresis loop of Fig. 6, which is found in good agreement with the experimental data. Although the value of J seems to be consistent ($J>T_{1/2}$), it important to remark that the shape and the width of the obtained hysteresis loop are model dependent. Indeed, going beyond the mean-field approach, by using Bethe-Peierls, cluster variational methods or Monte Carlo simulations will lead to a different value of the interaction parameter J. On the other hand, the probable existence of short- and long-range (elastic) interactions in the system lead to consider the obtained value of J as the lower limit value of the interaction strength. Therefore, the present model must be seen as a minimal model allowing to describe simply the cooperative Jahn-Teller transition in $RbMnFe(CN)_6$.

VI. CONCLUSION

Detailed studies of the thermal properties of ($RbMn[Fe(CN)_6]$) by means of SE have led to a complete understanding of the observed structural first-order transition in this cooperative Jahn-Teller system. This phase transition is accompanied by a metal-to-metal charge transfer from Mn^{II} to Fe^{III} and is coupled with a Jahn-Teller distortion of the produced Mn^{III} ion. Accumulating the SE spectra in heating and cooling modes, we derived a thermal hysteresis loop is from the analysis of the surface of the absorption spectra and found it in excellent agreement with that derived from magnetic measurements.

The spectra were fitted using GL line shape and the different contributions were assigned. Thus, in the LT phase, we have distinguished four oscillators, located at wavelengths 210, 457, 508, and 685 nm, corresponding, respectively, to the MLCT of $Fe^{2+}(CN)_6$, IT, and Mn^{3+} *d-d* JT transitions. In contrast, in the HT phase, we distinguished two oscillators at 220 and 405 nm, respectively, attributed to metal-to-metal (Fe-Mn) CT transitions. Remarkably, we also found that the thermal dependence of the oscillator strengths of the IT and Mn^{III} *d-d* bands show a bistable character in excellent agreement with that of magnetic measurements. We have also analyzed the thermal evolution of the energy shift the MLCT band (UV region), which expresses the change in symmetry of the lattice, and subsequent orbital overlapping. We have also established that it also constitutes a direct observation of the volume change with temperature. Indeed, the obtained relative change of energy $\Delta E/\bar{E}$ well correlates with the relative change in volume of the unit cell $\Delta V/\bar{V}$, which is derived from x-ray data. We then estimated the volumetric expansion factor in the LT and HT phases, as well as in the transition region, and the obtained results were found in very good agreement with available data in the literature.

In conclusion, this study demonstrates the relevance of the SE as a very accurate and nondestructive technique allowing to probe optical, mechanical, and thermodynamical properties of switchable photochromic solids. An extension of the present study including the investigations of the optical properties of the thermally quenched and the photoinduced metastable states by means of SE in also in progress.

ACKNOWLEDGMENTS

This work was supported by the "Ministère de l'Enseignement Supérieur et de la Recherche" (PPF contract), CNRS, Université de Versailles Saint-Quentin-en-Yvelines, France-Japan program GDRI No. 91, and Conseil Régional d'Ile de France. Acknowledgments are due to F. Varret (Versailles) for helpful discussions and a careful reading of the paper.

*kbo@physique.uvsq.fr

[1] O. Sato, J. Tao, and Y.-Z. Zhang, Angew. Chem., Int. Ed. **46**, 2152 (2007).
[2] O. Sato, T. Iyoda, A. Fujishima, and K. Hashimoto, Science **271**, 49 (1996).
[3] O. Sato, T. Iyoda, A. Fujishima, and K. Hashimoto, Science **272**, 704 (1996).
[4] S. Ferlay, T. Mallah, R. Ouahes, P. Veillet, and M. Verdaguer, Nature (London) **378**, 701 (1995).
[5] S. Ohkoshi, H. Tokoro, M. Utsunomiya, M. Mizuno, M. Abe, and K. Hashimoto, J. Phys. Chem. B **106**, 2423 (2002).
[6] H. Tokoro, T. Matsuda, K. Hashimoto, and S. Ohkoshi, J. Appl. Phys. **97**, 10M508 (2005).
[7] H. Tokoro, S. Ohkoshi, and K. Hashimoto, Appl. Phys. Lett. **82**, 1245 (2003).
[8] Y. Moritomo, A. Kuriki, K. Ohoyama, H. Tokoro, S. Ohkoshi, K. Hashimoto, and N. Hamada, J. Phys. Soc. Jpn. **72**, 456 (2003).
[9] K. Kato, Y. Moritomo, M. Takata, M. Sakata, M. Umekawa, N. Hamada, S. Ohkoshi, H. Tokoro, and K. Hashimoto, Phys. Rev. Lett. **91**, 255502 (2003).
[10] S. Margadonna, K. Prassides, and A. N. Fitch, Angew. Chem., Int. Ed. **43**, 6316 (2004).
[11] T. Nuida, T. Matsuda, H. Tokoro, S. Sakurai, K. Hashimoto, and S. Ohkoshi, J. Am. Chem. Soc. **127**, 11604 (2005).
[12] L. Egan, K. Kamenev, D. Papanikolaou, Y. Takabayashi, and S. Margadonna, J. Am. Chem. Soc. **128**, 6034 (2006).
[13] S. Ohkoshi, H. Tokoro, T. Matsuda, H. Takahashi, H. Irie, and K. Hashimoto, Angew. Chem., Int. Ed. **46**, 3238 (2007).
[14] P. N. Schatz, A. J. McCaffery, W. Suëtaka, G. N. Henning, A. B. Ritchie, and P. J. Stephens, J. Chem. Phys. **45**, 722 (1966).
[15] H. Tokoro, S. Ohkoshi, T. Matsuda, and K. Hashimoto, Inorg. Chem. **43**, 5231 (2004).
[16] S. Ohkoshi, H. Tokoro, and K. Hashimoto, Coord. Chem. Rev. **249**, 1830 (2005).
[17] H. Tokoro, S. Miyashita, K. Hashimoto, and S. Ohkoshi, Phys. Rev. B **73**, 172415 (2006).
[18] Y. Moritomo, K. Kato, A. Kuriki, M. Takata, M. Takara, M. Sakata, H. Tokoro, S. Ohkoshi, and K. Hashimoto, J. Phys. Soc. Jpn. **71**, 2078 (2002).
[19] H. Osawa, T. Iwzumi, H. Tokoro, S. Ohkoshi, K. Hashimoto, H. Shoji, E. Hirai, T. Nakamura, S. Nanao, and Y. Isozumi, Solid State Commun. **125**, 237 (2003).
[20] R. M. A. Azzam and N. M. Bashara, *Ellipsometry and Polarized Light* (North-Holland, Amsterdam, 1977).
[21] H. G. Tompkins and W. A. McGahan, *Spectroscopic Ellipsometry and Reflectometry* (Wiley, New York, 1999).
[22] H. G. Tompkins and E. A. Irene, *Handbook of Ellipsometry* (William Andrew Inc., Springer, New York, 2005).
[23] S. Ohkoshi, T. Nuida, T. Matsuda, H. Tokoro, and K. Hashimoto, J. Mater. Chem. **15**, 3291 (2005).
[24] E. D. Loutete-Dangui, F. Varret, E. Codjovi, P. R. Dahoo, H. Tokoro, S. Ohkoshi, C. Eypert, J. F. Létard, J. M. Coanga, and K. Boukheddaden, Phys. Rev. B **75**, 184425 (2007).
[25] B. Drevillon, J. Perrin, R. Marot, A. Violet, and J. L. Daldy, Rev. Sci. Instrum. **53**, 969 (1982).
[26] S. N. Jasperson and S. E. Schnatterly, Rev. Sci. Instrum. **40**, 761 (1969); S. N. Jasperson, D. K. Burge, and R. C. O'Handley, Surf. Sci. **37**, 548 (1973).
[27] G. R. Boyer, B. F. Lamouroux, and B. S. Prade, Appl. Opt. **18**, 1217 (1979).
[28] R. Kronig, J. Opt. Soc. Am. **12**, 547 (1926).
[29] H. A. Kramers, Nature (London) **117**, 775 (1926).
[30] R. Kronig, Ned. Tijdschr. Natuurkd. **9**, 402 (1942).
[31] H. A. Lorentz, *Versuch einer Theorie der Electrischen und Optischen Erscheinungen in Bewegten Koerpern* (Tuebner, Leipzig, 1906).
[32] H. A. Lorentz, *The Theory of Electrons* (Dover, New York, 1952).
[33] M. Born and K. Huang, *Dynamical Theory of Crystal Lattices* (Oxford University Press, New York, 1968).
[34] T. S. Davis, J. P. Fackeler, and M. J. Weeks, Inorg. Chem. **7**, 1994 (1968).
[35] S. Kück, S. Hartung, S. Hurling, K. Petermann, and G. Huber, Phys. Rev. B **57**, 2203 (1998).
[36] J. Humlíček, E. Schmidt, L. Bočánek, R. Švehla, and K. Ploog, Phys. Rev. B **48**, 5241 (1993).
[37] J. Humlicek, *Analysis of Spectrum Line Profiles*, Folia Fac. Sci. Nat. Univ. Brunensis Tomus XXV Physica Vol. 36, 1984 (unpublished).
[38] T. Kawamoto, Y. Asai, and S. Abe, Phys. Rev. Lett. **86**, 348 (2001).
[39] Y. Moritomo, K. Kato, A. Kuriki, M. Takata, M. Sakata, H. Tokoro, S. Ohkoshi, and K. Hashimoto, J. Phys. Soc. Jpn. **71**, 2078 (2002).
[40] F. H. Pollak, in *Strained-Layers Superlattices: Physics, Semiconductors, and Semimetals*, edited by T. P. Pearsall (Academic, London, 1992), Vol. 32, Chap. 2.
[41] T. Matsuda, H. Tokoro, K. Hashimoto, and S. Ohkoshi, Dalton Trans. **4**, 5046 (2006).
[42] S. Pillet, V. Legrand, M. Souhassou, and C. Lecomte, Phys. Rev. B **74**, 140101(R) (2006).
[43] S. Ohkoshi, T. Matsuda, H. Tokoro, and K. Hashimoto, Chem. Mater. **17**, 81 (2005).
[44] S. Miyashita, Y. Konishi, H. Tokoro, and M. Nishino, Prog. Theor. Phys. **114**, 719 (2005).
[45] H. Tokoro, S. Ohkoshi, T. Matsuda, T. Hozumi, and K. Hashimoto, Chem. Phys. Lett. **388**, 379 (2004).
[46] A. Sava, C. Enachescu, A. Stancu, K. Boukheddaden, E. Codjovi, I. Maurin, and F. Varret, J. Optoelectron. Adv. Mater. **5**, 977 (2003).
[47] M. Castro, K. Boukheddaden, F. Varret, H. Tokoro, and S. Ohkoshi (unpublished).
[48] K. Boukheddaden, I. Shteto, B. Hôo, and F. Varret, Phys. Rev. B **62**, 14806 (2000).
[49] K. Boukheddaden, M. Nishino, and S. Miyashita, Phys. Rev. Lett. **100**, 177206 (2008).